IEEE Access
Multidisciplinary | Rapid Review | Open Access Journal

Received April 4, 2020, accepted May 12, 2020, date of publication May 15, 2020, date of current version June 1, 2020.

Digital Object Identifier 10.1109/ACCESS.2020.2994976

Time Reversal Detection in Multistatic Radar System

ZHAOMING ZHANG, BAIXIAO CHEN, AND MINGLEI YANG, (Member, IEEE)
National Laboratory of Radar Signal Processing, Xidian University, Xi'an 710071, China

Corresponding author: Minglei Yang (mlyang@xidian.edu.com)

This work was supported in part by the National Natural Science Foundation of China under Grant 61571344 and Grant 6197010590, in part by the Fund for Foreign Scholars in University Research and Teaching Programs through the 111 Project under Grant B18039, and in part by the National Natural Science Foundation of Shaanxi Province under Grant 2017CGZH-RGXQ-02.

ABSTRACT A multistatic radar system can effectively improve the detection performance owing to its spatial diversity property. However, the detection performance will degrade when there exist multipaths. Time reversal has been proved to be able to transform the impact of the multipath into a favorable factor by matching propagation channels to achieve space-time focusing in a monostatic radar system. Therefore, we study the time reversal detection problem in a multistatic radar system with multipath environment in this paper. We divide the detection problems into two scenarios according to whether the channel response is known or not. In both scenarios, the time reversal detector and the conventional detector are derived respectively. Monte-Carlo experiments are used to examine the performance of the four detectors. The simulation results demonstrate that the time reversal detectors have a significant performance enhancement over the conventional detectors for the multistatic radar in a multipath environment, and more multipaths lead to better detection performance for the time reversal detectors. In addition, we also show that the detection probability improves with the increase of the number of radar transceivers.

INDEX TERMS Detection, multistatic radar, time reversal.

I. INTRODUCTION

Radar cross section (RCS), which affects the radar detection performance significantly, is associated with the radar observation angle. In a multistatic radar or a distributed multiple input multiple output (MIMO) radar, the target is illuminated from different directions to obtain spatial diversity which can overcome RCS fluctuation [1], [2]. Compared with the monostatic radar, the multistatic radar system utilizes spatial diversity to improve the detection performance [3]–[6]. There exist lots of multipaths for urban environments or low angle target detection [7], [8], which severely reduces the detection probability [9]. In order to solve the multipath problem in detection, the multistatic scattering model in multipath environment was studied [10]. However, it is difficult to build an accurate multipath channel model for a complex propagation environment. For the situation where the wide-sense noise covariance matrix is unknown, several detectors are derived by using a subspace model and assuming the persymmetric covariance structure [11]. In order to solve the signal mismatch caused by multipath, two selective detectors are proposed in [12]. In addition, a tunable detector [12] is studied to overcome the problem of worse robustness caused by selective detectors. In addition to reducing the adverse effects of multipath on detector performance, it is also a good idea to use multipath characteristics to improve detection results. In [13], according to the behavior of the multipath components, the prior knowledge of the environment is used to divide the environment into three different regions, each of which corresponds to a detector designed to improve detection performance. Another multipath exploiting adaptive radar which is called Multipath Adaptive Matched Filter, with the knowledge of the reflected steering vector for a known actual direct-path steering vector is devised in [14]. The diffuse multipath exploitation detectors are designed in [15] and [16] for point-like targets and range distributed targets, respectively. Besides exploiting multipath energy as in [14] and [15], multipath can also be utilized to increase spatial diversity. The adaptive OFDM radar is proposed to solve the problem of moving target detection in a multipath environment [17].

The time reversal (TR) [18] is a technique that can transform the influence of the multipaths into a favorable factor by matching the propagation channels. Its processing is shown

The associate editor coordinating the review of this manuscript and approving it for publication was Mehmet Alper Uslu.

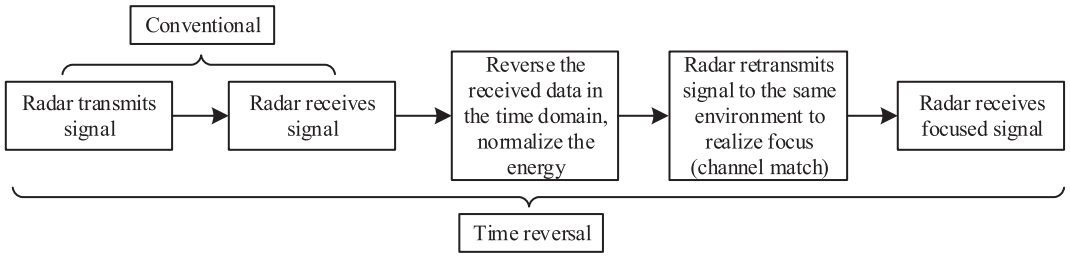

FIGURE 1. Configuration of time reversal process.

in Fig. 1. The radar receives the echo of a target as the conventional radar does first. Then, it forms the new transmitted signal by reversing the received data in the time domain (or by doing phase conjugation in the frequency domain) and normalizing energy. Subsequently, the new signal is transmitted to the target through the same scattering channel environment [18]. Owing to that the retransmitted signal is matched with the multipath propagation channel, it will refocus on the target with more energy than the first transmission. Finally, the radar receives the echoes of the target again, which is denoted as the time reversal echo. Therefore, time reversal does not require to construct the channel model in advance and it can effectively utilize multipaths to realize spatial and temporal focusing by matching channel response, which helps to improve the radar detection probability. And also more multipaths will bring more energy to the target, thus leading to better detection performance [19]. Time reversal was firstly proposed by Fink and applied to acoustics and ultrasound [20], [21], and then it is demonstrated to have a focusing effect on electromagnetic waves [22], [23]. Jin and Fink have done a lot of works on the detection problems using time reversal, such as the TR detection using a single antenna [24], antenna arrays [25]. Essentially, the radars in both papers are monostatic and do not have the advantage of spatial diversity. Then the time reversal detector in widely separated MIMO radar is introduced in [26]. However, the transmitted signals of each subarray or transmitter need to guarantee strict orthogonality for the MIMO radar to achieve channel separation by matched filtering. Therefore, to design the transmission waveform more flexibly without orthogonality, we extend the time reversal detection algorithm to a general multistatic radar system in this paper.

In the multistatic radar system, several spatially distributed transceivers are assumed. Each transceiver has one reciprocal antenna. We construct the signal for the multistatic radar and derive the TR detectors as well as conventional detectors. We consider two scenarios, the ideal case and the realistic case [24], [25], in which the channel response is known and unknown, respectively. In both scenarios, we derive the conventional detectors and the time reversal detectors, respectively. Under the ideal case, the time reversal transmitting signal is calculated according to the channel response. And we can analyse the detection probability, the false alarm probability and the detection threshold using the theoretical results. For the realistic scenario, the channel response is unknown. We estimate the channel response by applying a maximum likelihood method to the received signals. Then a generalized likelihood ratio test (GLRT) detector is derived to determine whether there is a target or not. We use Monte-Carlo experiments to analyse the detection performance of the detectors. Compared with the conventional detectors, the TR detectors obtain higher detection probabilities in both the ideal and the realistic cases.

The paper is organized as follows. Section II introduces the signal model including both the conventional one and the time reversal one, and analyses their statistical characteristics. Section III derives the conventional and time reversal detectors under the condition that the channel response is known and unknown, respectively. Section IV conducts simulation results and compares them with the theoretical results. Finally, Section V summarizes this paper.

*Notation:*Uppercase and lowercase blackface letters represent matrices and vectors, respectively. The symbol $(\cdot)^T$ stands for transpose; $(\cdot)^*$ denotes conjugate; $(\cdot)^H$ represents Hermitian transpose. The character $\sim$ is used to indicate statistical distribution. $\mathcal{CN}(\mu, \sigma^2)$ and $\mathcal{N}(\mu, \sigma^2)$ stand for complex Gaussian and Gaussian distributions with parameters μ and σ^2, respectively. Tr$(\cdot)$ represents the trace of the matrix. The symbol diag$(\cdot)$ represents a diagonal matrix whose diagonal elements are vectors in brackets. $\Re(\mathbf{x})$ is the real part of vector $\mathbf{x}$. The symbol $\mathbf{A}^+$ means Moore-Penrose inverse matrix of $\mathbf{A}$.

II. SIGNAL MODEL

A rich multipath environment is considered in this paper, such as low angle, indoor and urban scenes. We focus on the stationary or slow moving target detection problem of the multistatic radar system based on time reversal and ignore the clutters in this paper. But the multipaths cannot be eliminated because they are related to the target [27]. Hence, we consider the signal model that only includes the target echo and the multipaths. The target is stationary or moves slowly, therefore the Doppler frequency has little effect on target detection and we do not consider the Doppler frequency in the following analysis. We assume that the radar system is constructed by N distributed transceivers as shown in Fig. 2. All transceivers can both transmit and receive signals. Unlike the TR-MIMO radar, there is no need to ensure the orthogonality of

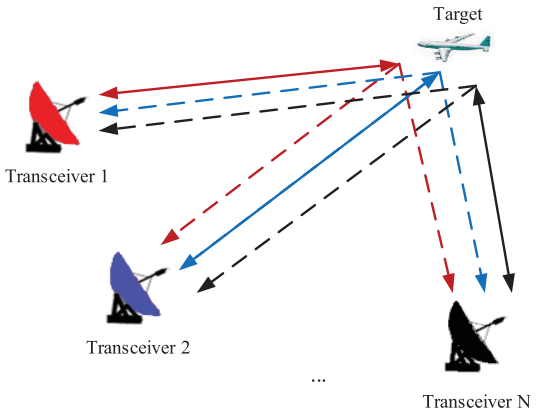

FIGURE 2. Configuration of a multistatic radar system.

transmitted signals to achieve channel separation by matched filtering in the multistatic radar. The transmitted wideband signal of each distributed transceiver is $f_n(t)$ and they have the same the timewidth T_p and the bandwidth B. The m-th discrete time domain sample of $f_n(t)$ is $f_n(m)$, $m = 0, \cdots, Q-1$. The discrete Fourier transform of $f_n(m)$ is $F_n(\omega_q)$, $\omega_q = q(B/(Q-1)) + \omega_{q_s}$, $q = 0, 1, \cdots, Q-1$ and ω_{q_s} is the starting frequency of signal, and $n = 1, \cdots, N$. The transmitted singal power of the n-th transceiver is $E_n = 1/Q \sum_{q=0}^{Q-1} |F_n(\omega_q)|^2$. The time reversal of transmitted signal is $f_n^*(-t)$, which the discrete sample is $f_n^*(-m)$. The discrete Fourier transform of $f_n^*(-m)$ is $F_n^*(\omega_q)$. Specially, for real-valued transmitted signal $f_n(-t) = f_n^*(-t)$, therefore the discrete Fourier transform of the time reversed signal corresponding to $f_n(m)$ is $F^*(\omega_q)$. Since rich multipaths cause difficulties for signal processing, in this article, we analyse signals in the frequency domain and consider the multipath effect as a channel as a whole, instead of considering the impact of each multipath on detection. Besides, according to the Parseval theorem, there is no energy loss when the signal is transformed from the time domain to the frequency domain. Hence, it is feasible to solve the problem in the frequency domain, which has been demonstrated by [19], [28], [29].

The channel response matrix at frequency ω_q is $\mathbf{H}(\omega_q)$, where the element $H_{ij}(\omega_q)$ represents the channel response from the j-th transmitter to the i-th receiver. Channel response is the product of two Green's functions. Let $G(\mathbf{r}, \mathbf{r}'; \omega_q)$ be the Green' function of the background medium between locations $\mathbf{r}'$ and $\mathbf{r}$ at frequency ω_q. The channel response is given by [30]

$$H_{ij}(\omega_q) = \tau(\mathbf{x}_t; \omega_q) G(\mathbf{x}_t, \mathbf{r}_j; \omega_q) G(\mathbf{r}_i, \mathbf{x}_t; \omega_q), \tag{1}$$

where $\tau(\mathbf{x}_t; \omega_q)$ is the complex reflectivity of the point target at location $\mathbf{x}_t$ and $\mathbf{r}_i$ is the location of the i-th transceiver. Because of the reciprocity relation of the Green's function, we obtain

$$G(\mathbf{r}, \mathbf{r}'; \omega_q) = G(\mathbf{r}', \mathbf{r}; \omega_q). \tag{2}$$

Since we assume that the target is stationary or moves slowly, the scattering environment can be considered unchanged, which results in $\mathbf{H}(\omega_q)$ being a symmetric matrix

$$H_{ij}(\omega_q) = H_{ji}(\omega_q), \quad \mathbf{H}(\omega_q) = \mathbf{H}^T(\omega_q). \tag{3}$$

The signal is processed in the frequency domain, hence channel $\mathbf{H}(\omega_q)$ for each frequency point ω_q is a superposition of all multipaths.

In order to show the advantages of time reversal target detection, we compare it with the conventional target detection. First, we give the conventional and time reversal signal models in this section.

A. CONVENTIONAL SIGNAL MODEL

For the l-th snapshot, $l = 1, \cdots, L$, being similar to the array antennas received signal in [25], the echo of n-th transceiver at frequency ω_q is $Y_{l,n}(\omega_q)$

$$Y_{l,n}(\omega_q) = \sum_{j=1}^{N} H_{n,j}(\omega_q) F_j(\omega_q) + V_{l,n}(\omega_q). \tag{4}$$

In this article, receiving one conventional echo is defined as one snapshot. The received signals of all N transceivers at the l-th snapshot and frequency ω_q are written in the form of $N \times 1$ dimensional vector

$$\begin{aligned} \mathbf{y}_l(\omega_q) &= [Y_{l,1}(\omega_q), \cdots, Y_{l,N}(\omega_q)]^T \\ &= \mathbf{H}(\omega_q)\boldsymbol{f}(\omega_q) + \mathbf{v}_l(\omega_q), \end{aligned} \tag{5}$$

$$\boldsymbol{f}(\omega_q) = [F_1(\omega_q), \cdots, F_N(\omega_q)]^T, \tag{6}$$

$$\mathbf{v}_l(\omega_q) = [V_{l,1}(\omega_q), \cdots, V_{l,N}(\omega_q)]^T, \tag{7}$$

where $\boldsymbol{f}(\omega_q)$ is the $N \times 1$ dimensional transmitted signal vector of N transceivers at frequency ω_q. $\mathbf{v}_l(\omega_q)$ is the noise vector of N transceivers at the l-th snapshot and frequency ω_q. $V_{l,n}(\omega_q)$ is the additive complex Gaussian white noise with zero mean and diagonal covariance σ_v^2. The received signals of the Q-th frequency points are stacked into $NQ \times 1$ dimensional vector, which represents a snapshot data

$$\begin{aligned} \mathbf{y}_l &= [\mathbf{y}_l^T(\omega_0), \cdots, \mathbf{y}_l^T(\omega_{Q-1})]^T \\ &= \mathbf{H}\boldsymbol{f} + \mathbf{v}_l, \end{aligned} \tag{8}$$

where

$$\mathbf{H} = \mathrm{diag}[\mathbf{H}(\omega_0), \cdots, \mathbf{H}(\omega_{Q-1})]_{NQ \times NQ}, \tag{9}$$

$$\boldsymbol{f} = [\boldsymbol{f}^T(\omega_0), \cdots, \boldsymbol{f}^T(\omega_{Q-1})]^T_{NQ \times 1}, \tag{10}$$

$$\mathbf{v}_l = [\mathbf{v}_l^T(\omega_0), \cdots, \mathbf{v}_l^T(\omega_{Q-1})]^T_{NQ \times 1}. \tag{11}$$

In (9), diagonal elements of $\mathbf{H}$ are block matrices.

Finally, L snapshots data are collected and written as $NQ \times L$ dimensional matrix

$$\mathbf{Y} = [\mathbf{y}_1, \cdots, \mathbf{y}_L]. \tag{12}$$

B. TR SIGNAL MODEL

The time reversal data are analysed on the basis of conventional received data. The received conventional signal of each transceiver for each snapshot is time reversed (or frequency domain conjugation), energy normalized, and retransmitted.

In the time reversal process, each time a conventional echo is received, and the corresponding time reversal echo is also received. However, these two echoes are uniformly called one snapshot. In other words, the snapshots of the time reversal and the conventional signal models are uniformly defined as the number of times of conventional signal $\mathbf{y}_l$ received. For the l-th snapshot, time reversal signal at frequency ω_q is given by

$$\begin{aligned}\mathbf{x}_l(\omega_q) &= \mathbf{H}(\omega_q)\mathbf{U}_l\mathbf{y}_l^*(\omega_q) + \mathbf{w}_l(\omega_q)\\ &= \mathbf{H}(\omega_q)\mathbf{U}_l\mathbf{H}^*(\omega_q)\boldsymbol{f}^*(\omega_q)\\ &\quad + \mathbf{H}(\omega_q)\mathbf{U}_l\mathbf{v}_l^*(\omega_q) + \mathbf{w}_l(\omega_q),\end{aligned} \tag{13}$$

where

$$\mathbf{U}_l = \text{diag}[u_{l,1}, \cdots, u_{l,N}]_{N\times N}, \tag{14}$$

$$\mathbf{w}_l(\omega_q) = [W_{l,1}(\omega_q), \cdots, W_{l,N}(\omega_q)]^T. \tag{15}$$

$u_{l,n}$ is the normalized factor of the n-th transceiver, l-th snapshot

$$u_{l,n} = \sqrt{\frac{\sum_{q=0}^{Q-1}|F_n(\omega_q)|^2}{\sum_{q=0}^{Q-1}|Y_{l,n}(\omega_q)|^2}}. \tag{16}$$

$u_{l,n}$ is used to ensure that the power of the time reversal transmitted signal is the same as the power of the conventional transmitted signal, i.e. E_n. Although the power of the received conventional echo $\mathbf{y}_l$ in each snapshot is different, the power of the time reversal transmitted signal remains the same after energy normalization. $W_{l,n}(\omega_q)$ is an additive circular complex zero mean white Gaussian noise with variance σ_w^2 of n-th transceiver received at the l-th snapshot.

$NQ \times 1$ dimensional vector of time reversal signal at l-th snapshot is described as

$$\mathbf{x}_l = \mathbf{H}\bar{\mathbf{U}}_l\mathbf{H}^*\boldsymbol{f}^* + \mathbf{H}\bar{\mathbf{U}}_l\mathbf{v}^* + \mathbf{w}_l, \tag{17}$$

$$\bar{\mathbf{U}}_l = \text{diag}[\mathbf{U}_l, \cdots, \mathbf{U}_l]_{NQ\times NQ}, \tag{18}$$

$$\mathbf{w}_l = [\mathbf{w}_l^T(\omega_0), \cdots, \mathbf{w}_l^T(\omega_{Q-1})]^T. \tag{19}$$

Just like [25], for the TR target detection, $\mathbf{y}_l^*$ and $\mathbf{x}_l$ are combined to get more information

$$\mathbf{z}_l = \begin{bmatrix}(\mathbf{y}_l^*)^T & \mathbf{x}_l^T\end{bmatrix}^T. \tag{20}$$

Similar to (12), all received data can be written as a matrix $\mathbf{Z}$, which is defined as

$$\mathbf{Z} = [\mathbf{z}_1, \cdots, \mathbf{z}_L]. \tag{21}$$

C. STATISTICAL CHARACTERISTIC

In this section, we analyse the statistical properties of the time reversal and the conventional signals. Because $V_{l,n}(\omega_q)$ and $W_{l,n}(\omega_q)$ satisfy complex Gaussian distribution, hence $\mathbf{v}_l$ and $\mathbf{w}_l$ are circular complex Gaussian random vectors

$$\mathbf{v}_l \sim \mathcal{CN}(0, \sigma_v^2\mathbf{I}_{NQ}), \tag{22}$$

$$\mathbf{w}_l \sim \mathcal{CN}(0, \sigma_w^2\mathbf{I}_{NQ}). \tag{23}$$

Note that $\mathbf{v}_l$ and $\mathbf{w}_l$ are the additive complex white Gaussian noise of the conventional and the time reversed received signal, respectively. In the time reversal step, the conventional received signal is transmitted first, which including noise $\mathbf{v}_l$. $\mathbf{v}_l$ and $\mathbf{w}_l$ are independent of the target response and on the other hand, they are statistically independent. Based on this statistical characteristic, the received signals satisfy

$$\mathbf{y}_l \sim \mathcal{CN}(\mathbf{H}\boldsymbol{f}, \sigma_v^2\mathbf{I}_{NQ}), \tag{24}$$

$$\mathbf{x}_l \sim \mathcal{CN}(\mathbf{H}\bar{\mathbf{U}}\mathbf{H}^*\boldsymbol{f}^*, \sigma_v^2\mathbf{H}\bar{\mathbf{U}}\bar{\mathbf{U}}\mathbf{H}^H + \sigma_w^2\mathbf{I}_{NQ}). \tag{25}$$

III. DETECTORS

In this subsection, binary hypothesis test is used for the TR detection and the conventional detection problems. Under the null hypothesis $\mathbb{H}_0$, there is no target while under the hypothesis $\mathbb{H}_1$ the target signal exists. For these detection problems, we consider two scenarios [24], [25]. One is defined as the ideal scenario where channel response $\mathbf{H}$ is known. And the other is referred to as the realistic scenario where channel response $\mathbf{H}$ is unknown. For both the ideal and the realistic scenarios, the main difference is whether the channel response is known or not, which leads to different detectors. When designing the ideal detectors, the channel response can be considered constant because it is known. For the realistic detectors, since the channel response is unknown, the maximum likelihood (ML) estimation of the channel response is needed when designing the generalized likelihood ratio test (GLRT) detectors. In the following, four detectors are described in detail:

1) the conventional detector with known channel response (short as ideal-CD)

2) the time reversal detector with known channel response (short as ideal-TR)

3) the conventional detector with unknown channel response (short as CD-GLRT)

4) the time reversal detector with unknown channel response (short as TR-GLRT)

In the conventional detection method, a binary hypothesis test is directly performed on the received echo, and multipath information is not exploited, which often reduces the performance of the detector and increases the false alarm rate. In contrast, although the time reversal detection method also uses a binary hypothesis test, the time reversal echo is a signal after spatial and temporal focusing, that is, channel matching is achieved and multipath information is exploited.

A. CONVENTIONAL DETECTOR WITH KNOWN CHANNEL RESPONSE

For the ideal conventional detection problem, the binary hypothesis test, the false alarm probability and the detection probability are derived. The binary hypothesis test is given by

$$\begin{aligned}\mathbb{H}_1 &: \mathbf{y}_l = \mathbf{H}\boldsymbol{f} + \mathbf{v}_l\\ \mathbb{H}_0 &: \mathbf{y}_l = \mathbf{v}_l.\end{aligned} \tag{26}$$

In this scenario, $\mathbf{H}$ is known, and on the other hand, $\mathbf{y}_l$ satisfies complex Gaussian distribution based on (24). The probability

density functions (pdfs) under hypothesis $\mathbb{H}_1$ and $\mathbb{H}_0$ are

$$p(\mathbf{Y}|\mathbb{H}_1) = \frac{1}{(\pi\sigma_v^2)^{NQL}} \exp\Big\{ -\sum_{l=1}^{L} \frac{||\mathbf{y}_l - \mathbf{H}\boldsymbol{f}||^2}{\sigma_v^2} \Big\}, \tag{27}$$

$$p(\mathbf{Y}|\mathbb{H}_0) = \frac{1}{(\pi\sigma_v^2)^{NQL}} \exp\Big\{ -\sum_{l=1}^{L} \frac{||\mathbf{y}_l||^2}{\sigma_v^2} \Big\}. \tag{28}$$

The likelihood ratio can be obtained by dividing (27) with (28)

$$\ell(\mathbf{Y}) = \frac{p(\mathbf{Y}|\mathbb{H}_1)}{p(\mathbf{Y}|\mathbb{H}_0)}. \tag{29}$$

Then we take the logarithm of (29) and discard the constant terms. And since channel response $\mathbf{H}$ is known, the logarithm result of (29) can be normalized with $2\sigma_v||\mathbf{H}\boldsymbol{f}||$, which is a constant being calculated in advance. The likelihood ratio test of conventional ideal detector is

$$\ell_{\text{ideal-CD}}(\mathbf{Y}) = \Re\Big\{ \frac{(\mathbf{H}\boldsymbol{f})^H \sum_{l=1}^{L} \mathbf{y}_l}{\sigma_v||\mathbf{H}\boldsymbol{f}||} \Big\}. \tag{30}$$

In the ideal scenario, $\mathbf{H}$ and $\boldsymbol{f}$ are determined. Under hypothesis $\mathbb{H}_0$, $\mathbf{y}_l = \mathbf{v}_l$, and $\mathbf{v}_l$ is distributed as in (22). $\ell_{\text{ideal-CD}}$ is a complex random variable. It is straightforward to know

$$\Big(\frac{(\mathbf{H}\boldsymbol{f})^H \sum_{l=1}^{L} \mathbf{v}_l}{\sigma_v||\mathbf{H}\boldsymbol{f}||} \Big) \sim \mathcal{CN}(0, L), \tag{31}$$

$$\ell_{\text{ideal-CD}}(\mathbf{Y}) \sim \mathcal{N}(0, \frac{L}{2}). \tag{32}$$

The false alarm probability $P_{fa,\text{CD}}$ is obtained by integrating $\ell_{\text{ideal-CD}}$ from threshold to infinity under $\mathbb{H}_0$

$$\begin{aligned} P_{fa,\text{CD}} &= \int_{\eta_{\text{CD}}}^{\infty} \frac{1}{\sqrt{2\pi L/2}} e^{-\frac{x^2}{2L/2}} dx \\ &= \int_{\frac{\eta_{\text{CD}}}{\sqrt{L}}}^{\infty} \frac{1}{\sqrt{\pi}} e^{-x^2} dx \\ &= \frac{1}{2}\Big(1 - \text{erf}\Big(\frac{\eta_{\text{CD}}}{\sqrt{L}}\Big)\Big) \end{aligned} \tag{33}$$

$$\eta_{\text{CD}} = \sqrt{L}\text{erf}^{-1}(1 - 2P_{fa}), \tag{34}$$

where η_{CD} is the detection threshold. $\text{erf}(\cdot)$ is the error function and $\text{erf}^{-1}(\cdot)$ is the inverse error function.

Under hypothesis $\mathbb{H}_1$, the received data consist of the target signal and noise. The test statistic $\ell_{\text{ideal-CD}}(\mathbf{Y})$ is equivalent to

$$\begin{aligned} \ell_{\text{ideal-CD}}(\mathbf{Y}) &= \Re\Big\{ \frac{(\mathbf{H}\boldsymbol{f})^H \sum_{l=1}^{L} (\mathbf{H}\boldsymbol{f} + \mathbf{v}_l)}{\sigma_v||\mathbf{H}\boldsymbol{f}||} \Big\} \\ &= L\frac{||\mathbf{H}\boldsymbol{f}||}{\sigma_v} + \Re\Big\{ \frac{(\mathbf{H}\boldsymbol{f})^H \sum_{l=1}^{L} \mathbf{v}_l}{\sigma_v||\mathbf{H}\boldsymbol{f}||} \Big\} \\ &= \mu_{\text{CD}} + \Re\Big\{ \frac{(\mathbf{H}\boldsymbol{f})^H \sum_{l=1}^{L} \mathbf{v}_l}{\sigma_v||\mathbf{H}\boldsymbol{f}||} \Big\}, \end{aligned} \tag{35}$$

where μ_{CD} is the mean value

$$\mu_{\text{CD}} = L\frac{||\mathbf{H}\boldsymbol{f}||}{\sigma_v}. \tag{36}$$

The probability density function of the test statistic $\ell_{\text{ideal-CD}}(\mathbf{Y})$ under $\mathbb{H}_1$ is

$$\ell_{\text{ideal-CD}}(\mathbf{Y}) \sim \mathcal{N}(\mu_{\text{CD}}, \frac{L}{2}). \tag{37}$$

The detection probability $P_{d,\text{CD}}$ is

$$\begin{aligned} P_{d,\text{CD}} &= \int_{\eta_{\text{CD}}}^{\infty} \frac{1}{\sqrt{2\pi L/2}} e^{-\frac{(x-\mu_{\text{CD}})^2}{2L/2}} dx \\ &= \frac{1}{2}\Big(1 - \text{erf}\Big(\frac{\eta_{\text{CD}} - \mu_{\text{CD}}}{\sqrt{L}}\Big)\Big). \end{aligned} \tag{38}$$

B. TIME REVERSAL DETECTOR WITH KNOWN CHANNEL RESPONSE

In this section, the binary hypothesis test, the false alarm probability and the detection probability about ideal time reversal detection problem are derived.

It is straightforward to compute the transmitted signal of time reversal because $\mathbf{H}$ is known. The essence of time reversal is channel matching. Under the ideal scenario, the channel response is known, so it is not necessary to transmit $\boldsymbol{f}$ to obtain the channel information, just to transmit $\mathbf{H}\boldsymbol{f}$ directly. $\mathbf{v}_l$ is assumed to be zero, i.e., conventional transmitting is considered a virtual transmitting. The conventional received signal of the l-th snapshot, the n-th transceiver is

$$Y_{l,n}(\omega_q) = \sum_{j=1}^{N} H_{n,j}(\omega_q) F_j(\omega_q). \tag{39}$$

Without noise $\mathbf{v}_l$, the normalized factor $u_{l,n}$ of each snapshot is equal to

$$u_{l,n} \equiv u_n = \sqrt{\frac{\sum_{q=0}^{Q-1} |F_n(\omega_q)|^2}{\sum_{q=0}^{Q-1} |Y_{l,n}(\omega_q)|^2}}, \tag{40}$$

$$\mathbf{U}_l \equiv \mathbf{U} = \text{diag}[u_1, \cdots, u_N], \tag{41}$$

$$\bar{\mathbf{U}}_l \equiv \bar{\mathbf{U}} = \text{diag}[\mathbf{U}, \cdots, \mathbf{U}]. \tag{42}$$

For the ideal TR detection problem, the binary hypothesis test is given by

$$\begin{aligned} \mathbb{H}_1 &: \mathbf{x}_l = \mathbf{H}\bar{\mathbf{U}}\mathbf{H}^*\boldsymbol{f}^* + \mathbf{w}_l \\ \mathbb{H}_0 &: \mathbf{x}_l = \mathbf{w}_l. \end{aligned} \tag{43}$$

The data pdfs under $\mathbb{H}_1$ and $\mathbb{H}_0$ are, respectively

$$p(\mathbf{X}|\mathbb{H}_1) = \frac{1}{(\pi\sigma_w^2)^{NQL}} \exp\Big\{ -\sum_{l=1}^{L} \frac{||\mathbf{x}_l - \mathbf{H}\bar{\mathbf{U}}\mathbf{H}^*\boldsymbol{f}^*||^2}{\sigma_w^2} \Big\}, \tag{44}$$

$$p(\mathbf{X}|\mathbb{H}_0) = \frac{1}{(\pi\sigma_w^2)^{NQL}} \exp\Big\{ -\sum_{l=1}^{L} \frac{||\mathbf{x}_l||^2}{\sigma_w^2} \Big\}. \tag{45}$$

The likelihood ratio is derived by dividing (44) with (45), then taking the logarithm of the result, ignoring the known constant terms, finally, normalizing the result with $2\sigma_w||\mathbf{H}\bar{\mathbf{U}}\mathbf{H}^*\boldsymbol{f}^*||$

$$\ell_{\text{ideal-TR}}(\mathbf{X}) = \Re\Big\{ \frac{(\mathbf{H}\bar{\mathbf{U}}\mathbf{H}^*\boldsymbol{f}^*)^H \sum_{l=1}^{L} \mathbf{x}_l}{\sigma_w||\mathbf{H}\bar{\mathbf{U}}\mathbf{H}^*\boldsymbol{f}^*||} \Big\}. \tag{46}$$

Under hypothesis $\mathbb{H}_0$, the received signal is noise, $\mathbf{x}_l = \mathbf{w}_l$, and $\mathbf{x}_l$ is a complex Gaussian random vector. On the other hand, $\mathbf{H}$, $\overline{\mathbf{U}}$ and $\boldsymbol{f}$ are known and determined, which can be assumed constant. Hence $\ell_{\text{ideal-TR}}(\mathbf{X})$ is a random variable

$$\left(\frac{(\mathbf{H}\overline{\mathbf{U}}\mathbf{H}^*\boldsymbol{f}^*)^H \sum_{l=1}^{L}\mathbf{w}_l}{\sigma_w||\mathbf{H}\overline{\mathbf{U}}\mathbf{H}^*\boldsymbol{f}^*||}\right) \sim \mathcal{CN}(0, L), \tag{47}$$

$$\ell_{\text{ideal-TR}}(\mathbf{X}) \sim \mathcal{N}(0, \frac{L}{2}). \tag{48}$$

The false alarm probability of TR detection $P_{fa,\text{TR}}$ is obtained by integrating $\ell_{\text{ideal-TR}}(\mathbf{X})$ from threshold η_{TR} to infinity under hypothesis $\mathbb{H}_0$

$$\begin{aligned} P_{fa,\text{TR}} &= \int_{\eta_{\text{TR}}}^{\infty} \frac{1}{\sqrt{2\pi L/2}} e^{-\frac{x^2}{2L/2}} dx \\ &= \int_{\frac{\eta_{\text{TR}}}{\sqrt{L}}}^{\infty} \frac{1}{\sqrt{\pi}} e^{-x^2} dx \\ &= \frac{1}{2}\left(1 - \text{erf}\left(\frac{\eta_{\text{TR}}}{\sqrt{L}}\right)\right), \end{aligned} \tag{49}$$

$$\eta_{\text{TR}} = \sqrt{L}\text{erf}^{-1}(1 - 2P_{fa}). \tag{50}$$

Under hypothesis $\mathbb{H}_1$, the received data consist of the target signal and noise. The test statistic $\ell_{\text{ideal-TR}}(\mathbf{X})$ is equivalent to

$$\begin{aligned} &\ell_{\text{ideal-TR}}(\mathbf{X}) \\ &= \Re\left\{\frac{(\mathbf{H}\overline{\mathbf{U}}\mathbf{H}^*\boldsymbol{f}^*)^H \sum_{l=1}^{L}(\mathbf{H}\overline{\mathbf{U}}\mathbf{H}^*\boldsymbol{f}^* + \mathbf{w}_l)}{\sigma_w||\mathbf{H}\overline{\mathbf{U}}\mathbf{H}^*\boldsymbol{f}^*||}\right\} \\ &= L\frac{||\mathbf{H}\overline{\mathbf{U}}\mathbf{H}^*\boldsymbol{f}^*||}{\sigma_w} + \Re\left\{\frac{(\mathbf{H}\overline{\mathbf{U}}\mathbf{H}^*\boldsymbol{f}^*)^H \sum_{l=1}^{L}\mathbf{w}_l}{\sigma_w||\mathbf{H}\overline{\mathbf{U}}\mathbf{H}^*\boldsymbol{f}^*||}\right\} \\ &= \mu_{\text{TR}} + \Re\left\{\frac{(\mathbf{H}\overline{\mathbf{U}}\mathbf{H}^*\boldsymbol{f}^*)^H \sum_{l=1}^{L}\mathbf{w}_l}{\sigma_w||\mathbf{H}\overline{\mathbf{U}}\mathbf{H}^*\boldsymbol{f}^*||}\right\}, \end{aligned} \tag{51}$$

where μ_{TR} is the mean value

$$\mu_{\text{TR}} = L\frac{||\mathbf{H}\overline{\mathbf{U}}\mathbf{H}^*\boldsymbol{f}^*||}{\sigma_w}. \tag{52}$$

Compared with (36), although $\boldsymbol{f}$ and $\overline{\mathbf{U}}\mathbf{H}^*\boldsymbol{f}^*$ have the same power, μ_{CD} and μ_{TR} are different, even if σ_v is equal to σ_w. Since it is not guaranteed that each corresponding element of $\boldsymbol{f}$ and $\overline{\mathbf{U}}\mathbf{H}^*\boldsymbol{f}^*$ is always the same.

The probability density function of the $\ell_{\text{ideal-TR}}(\mathbf{X})$ under hypothesis $\mathbb{H}_1$ is

$$\ell_{\text{ideal-TR}}(\mathbf{X}) \sim \mathcal{N}(\mu_{\text{TR}}, \frac{L}{2}). \tag{53}$$

The detection probability is given by

$$\begin{aligned} P_{d,\text{TR}} &= \int_{\eta_{\text{TR}}}^{\infty} \frac{1}{\sqrt{2\pi L/2}} e^{-\frac{(x-\mu_{\text{TR}})^2}{2\pi L/2}} dx \\ &= \frac{1}{2}\left(1 - \text{erf}\left(\frac{\eta_{\text{TR}} - \mu_{\text{TR}}}{\sqrt{L}}\right)\right). \end{aligned} \tag{54}$$

C. CONVENTIONAL DETECTOR WITH UNKNOWN CHANNEL RESPONSE

In the realistic conventional scenario, the channel response $\mathbf{H}$ is unknown, which is obtained by maximum likelihood estimation. The detection problem is equivalent to a conventional detection generalized likelihood ratio test problem (CD-GLRT). The binary hypothesis test for the realistic conventional detection is derived in the following.

In the realistic case, the detection problem is similar to (26), except $\mathbf{H}$ is unknown while $\mathbf{H}$ is assumed known in the ideal scenario. Then the generalized likelihood ratio test is derived. The pdfs $p(\mathbf{Y}|\mathbb{H}_1)$ and $p(\mathbf{Y}|\mathbb{H}_0)$ are given by

$$\begin{aligned} p(\mathbf{Y}|\mathbb{H}_1) = &\prod_{q=0}^{Q-1} \frac{1}{(\pi\sigma_v^2)^{NL}} \\ &\times \exp\left\{-\sum_{l=1}^{L}\frac{||\mathbf{y}_l(\omega_q) - \mathbf{H}(\omega_q)\boldsymbol{f}(\omega_q)||^2}{\sigma_v^2}\right\}, \end{aligned} \tag{55}$$

$$p(\mathbf{Y}|\mathbb{H}_0) = \prod_{q=0}^{Q-1} \frac{1}{(\pi\sigma_v^2)^{NL}} \exp\left\{-\sum_{l=1}^{L}\frac{||\mathbf{y}_l(\omega_q)||}{\sigma_v^2}\right\}. \tag{56}$$

Generalized likelihood ratio test is used in this detection problem. Unlike (30), here the constant term $||\mathbf{H}(\omega_q)\boldsymbol{f}(\omega_q)||$ cannot be discarded because of unknown $\mathbf{H}$. In (29), the numerator and the denominator are replaced by (55) and (56), respectively. Then taking the logarithm of the result in (29) and discarding the constant terms, the test statistic is given by

$$\begin{aligned} \ell_{\text{CD-GLRT}}(\mathbf{Y}) &= \ln p(\mathbf{Y}|\mathbb{H}_1) - \ln p(\mathbf{Y}|\mathbb{H}_0) \\ &= \frac{1}{\sigma_v^2}\sum_{l=1}^{L}\sum_{q=0}^{Q-1}\Big\{||\mathbf{y}_l(\omega_q)||^2 \\ &\quad - ||\mathbf{y}_l(\omega_q) - \mathbf{H}(\omega_q)\boldsymbol{f}(\omega_q)||^2\Big\} \\ &= \frac{1}{\sigma_v^2}\sum_{l=1}^{L}\sum_{q=0}^{Q-1}\Big\{2\Re[\mathbf{y}_l^H(\omega_q)\mathbf{H}(\omega_q)\boldsymbol{f}(\omega_q)] \\ &\quad - ||\mathbf{H}(\omega_q)\boldsymbol{f}(\omega_q)||^2\Big\} \\ &= \frac{1}{\sigma_v^2}\sum_{q=0}^{Q-1}\Big\{2\Re\{\text{Tr}[\mathbf{H}^H(\omega_q)\mathbf{B}(\omega_q)]\} \\ &\quad - \text{Tr}[\mathbf{H}^H(\omega_q)\mathbf{H}(\omega_q)\mathbf{A}(\omega_q)]\Big\}, \end{aligned} \tag{57}$$

where

$$\mathbf{A}(\omega_q) = L\boldsymbol{f}(\omega_q)\boldsymbol{f}^H(\omega_q), \tag{58}$$

$$\mathbf{B}(\omega_q) = \sum_{l=1}^{L}\mathbf{y}_l(\omega_q)\boldsymbol{f}^H(\omega_q). \tag{59}$$

Because of the unknown channel response $\mathbf{H}(\omega_q)$, the maximum likelihood estimation $\hat{\mathbf{H}}(\omega_q)$ is obtained by taking the partial derivative of $\ln p(\mathbf{Y}|\mathbb{H}_1)$ with respect to $\mathbf{H}^*(\omega_q)$

$$\frac{\partial \ln[p(\mathbf{Y}|\mathbb{H}_1)]}{\partial \mathbf{H}^*(\omega_q)}$$

$$= \frac{\partial}{\partial \mathbf{H}^*(\omega_q)} \sum_{l=1}^{L} \sum_{q=0}^{Q-1} \frac{1}{\sigma_v^2} \Big\{ - ||\mathbf{y}_l(\omega_q)||^2 - ||\mathbf{H}(\omega_q)\boldsymbol{f}(\omega_q)||^2 + 2\Re\{\mathbf{y}_l(\omega_q)\mathbf{H}(\omega_q)\boldsymbol{f}(\omega_q)\} \Big\}$$
$$= \frac{\partial}{\partial \mathbf{H}^*(\omega_q)} \sum_{q=0}^{Q-1} \frac{1}{\sigma_v^2} \Big\{ - ||\mathbf{y}_l(\omega_q)||^2 - \mathrm{Tr}[\mathbf{H}^H(\omega_q)\mathbf{H}(\omega_q)\mathbf{A}(\omega_q)] + 2\Re\{\mathrm{Tr}[\mathbf{H}^H(\omega_q)\mathbf{B}(\omega_q)]\} \Big\}. \quad (60)$$

According to the conjugate gradient of trace function [31]

$$\frac{\partial \mathrm{Tr}(\boldsymbol{R}^H \boldsymbol{T})}{\partial \boldsymbol{R}^*} = \boldsymbol{T}, \quad (61)$$

(60) is equivalent to

$$\frac{\partial \ln[p(\mathbf{Y}|\mathbb{H}_1)]}{\partial \mathbf{H}^*(\omega_q)} = \mathbf{B}(\omega_q) - \mathbf{H}(\omega_q)\mathbf{A}(\omega_q). \quad (62)$$

The maximum likelihood estimation $\hat{\mathbf{H}}(\omega_q)$ is calculated by letting (62) equal to zero

$$\hat{\mathbf{H}}(\omega_q) = \mathbf{B}(\omega_q)\mathbf{A}^{+}(\omega_q). \quad (63)$$

Finally, the channel response estimation $\hat{\mathbf{H}}$ is obtained

$$\hat{\mathbf{H}} = \mathrm{diag}[\hat{\mathbf{H}}(\omega_q), \cdots, \hat{\mathbf{H}}(\omega_q)]. \quad (64)$$

Unlike the ideal conventional detector, it is difficult to analyse the theoretical values of the detection probability and the false alarm probability according to the test statistic $\ell_{\text{CD-GLRT}}$, and therefore the Monte-Carlo experiments are used to study the detector performance in the following analysis in section IV.

D. TIME REVERSAL DETECTOR WITH UNKNOWN CHANNEL RESPONSE

In this scenario, the time reversal generalized likelihood ratio test (TR-GLRT) is used to solve the detection problem with $\hat{\mathbf{H}}(\omega_q)$ obtained by maximum likelihood estimation.

The time reversal detection problem is

$$\mathbb{H}_1 : \mathbf{z}_l = \begin{bmatrix} \mathbf{H}^*\boldsymbol{f}^* \\ \mathbf{H}\overline{\mathbf{U}}_l\mathbf{H}^*\boldsymbol{f}^* \end{bmatrix} + \begin{bmatrix} \mathbf{v}^* \\ \mathbf{H}\overline{\mathbf{U}}_l\mathbf{v}^* + \mathbf{w} \end{bmatrix}$$
$$\mathbb{H}_0 : \mathbf{z}_l = \begin{bmatrix} \mathbf{v}^* \\ \mathbf{w} \end{bmatrix}. \quad (65)$$

Next, the pdfs under $\mathbb{H}_1$ and $\mathbb{H}_0$ are derived. The covariance matrix of $\mathbf{z}_l(\omega_q)$ is

$$\boldsymbol{\Lambda}(q) = \begin{bmatrix} \sigma_v^2\mathbf{I}_N & \sigma_v^2\mathbf{U}_l\mathbf{H}^H(\omega_q) \\ \sigma_v^2\mathbf{H}(\omega_q)\mathbf{U}_l & \sigma_v^2\mathbf{H}(\omega_q)\mathbf{U}_l^2\mathbf{H}^H(\omega_q) + \sigma_w^2\mathbf{I}_N \end{bmatrix}. \quad (66)$$

According to the inversion criterion of block matrices and formula for determinants of block matrices [31], the inverse matrix and the determinant of $\boldsymbol{\Lambda}(q)$ are given by

$$\boldsymbol{\Lambda}^{-1}(q) = \begin{bmatrix} \frac{1}{\sigma_v^2}\mathbf{I}_N + \frac{1}{\sigma_w^2}\mathbf{U}_l\mathbf{H}^H(\omega_q)\mathbf{H}(\omega_q)\mathbf{U}_l & -\frac{1}{\sigma_w^2}\mathbf{U}_l\mathbf{H}^H(\omega_q) \\ -\frac{1}{\sigma_w^2}\mathbf{H}(\omega_q)\mathbf{U}_l & \frac{1}{\sigma_w^2}\mathbf{I}_N \end{bmatrix}, \quad (67)$$

$$|\boldsymbol{\Lambda}(q)| = |\sigma_v^2\mathbf{I}_N||\sigma_w^2\mathbf{I}_N| = (\sigma_v^2\sigma_w^2)^N. \quad (68)$$

The pdfs $p(\mathbf{Z}|\mathbb{H}_1)$ and $p(\mathbf{Z}|\mathbb{H}_0)$ are given by

$$p(\mathbf{Z}|\mathbb{H}_1) = \prod_{q=0}^{Q-1} \frac{1}{(\pi|\boldsymbol{\Lambda}(q)|)^L} \exp\Big\{ - \sum_{l=1}^{L} \begin{bmatrix} \mathbf{y}_l^* - \mathbf{H}^*(\omega_q)\boldsymbol{f}^*(\omega_q) \\ \mathbf{x}_l(\omega_q) - \mathbf{H}(\omega_q)\mathbf{U}_l\mathbf{H}^*(\omega_q)\boldsymbol{f}^*(\omega_q) \end{bmatrix}^H \boldsymbol{\Lambda}^{-1}(q) \begin{bmatrix} \mathbf{y}_l^* - \mathbf{H}^*(\omega_q)\boldsymbol{f}^*(\omega_q) \\ \mathbf{x}_l(\omega_q) - \mathbf{H}(\omega_q)\mathbf{U}_l\mathbf{H}^*(\omega_q)\boldsymbol{f}^*(\omega_q) \end{bmatrix} \Big\}$$
$$= \prod_{q=0}^{Q-1} \frac{1}{(\pi|\boldsymbol{\Lambda}(q)|)^L} \exp\Big\{ \sum_{l=1}^{L} - \frac{||\mathbf{y}_l(\omega_q)||^2}{\sigma_v^2} - \frac{||\mathbf{x}_l(\omega_q)||^2}{\sigma_w^2} + 2\Re\Big\{ \frac{\mathbf{y}_l^T(\omega_q)\mathbf{H}^*(\omega_q)\boldsymbol{f}^*(\omega_q)}{\sigma_v^2} + \frac{\mathbf{y}_l^T(\omega_q)\mathbf{U}_l\mathbf{H}^H(\omega_q)\boldsymbol{f}(\omega_q)}{\sigma_w^2} \Big\} - \frac{||\mathbf{H}^*(\omega_q)\boldsymbol{f}^*(\omega_q)||^2}{\sigma_v^2} - \frac{||\mathbf{H}(\omega_q)\mathbf{U}_l\mathbf{y}_l^*(\omega_q)||^2}{\sigma_w^2} \Big\}, \quad (69)$$

$$p(\mathbf{Z}|\mathbb{H}_0) = \prod_{q=0}^{Q-1} \frac{1}{\pi^L(\sigma_v^2\sigma_w^2)^{NL}} \exp\Big\{ - \sum_{l=1}^{L} \frac{||\mathbf{y}_l(\omega_q)||^2}{\sigma_v^2} \Big\} \times \exp\Big\{ - \sum_{l=1}^{L} \frac{||\mathbf{x}_l(\omega_q)||^2}{\sigma_w^2} \Big\}. \quad (70)$$

Take the logarithm of (69) and (70), respectively, and the test statistic is derived by $\ln p(\mathbf{Z}|\mathbb{H}_1) - \ln p(\mathbf{Z}|\mathbb{H}_0)$ with the maximum likelihood estimation of $\hat{\mathbf{H}}(\omega_q)$

$$\ell_{\text{TR-GLRT}}(\mathbf{Z}) = \ln p(\mathbf{Z}|\mathbb{H}_1) - \ln p(\mathbf{Z}|\mathbb{H}_0)$$
$$= \sum_{q=0}^{Q-1} \sum_{l=1}^{L} \Big\{ 2\Re\Big\{ \frac{\mathbf{y}_l^T(\omega_q)\hat{\mathbf{H}}^*(\omega_q)\boldsymbol{f}^*(\omega_q)}{\sigma_v^2} + \frac{\mathbf{y}_l^T(\omega_q)\mathbf{U}_l\hat{\mathbf{H}}^H(\omega_q)\mathbf{x}_l(\omega_q)}{\sigma_w^2} \Big\} - \frac{||\hat{\mathbf{H}}^*(\omega_q)\boldsymbol{f}^*(\omega_q)||^2}{\sigma_v^2} - \frac{||\hat{\mathbf{H}}(\omega_q)\mathbf{U}_l\mathbf{y}_l^*(\omega_q)||^2}{\sigma_w^2} \Big\}$$

$$= \sum_{q=0}^{Q-1} \Big\{ 2\Re\Big\{ \mathrm{Tr}[\hat{\mathbf{H}}^H(\omega_q)\mathbf{A}(\omega_q)] + \mathrm{Tr}[\hat{\mathbf{H}}^*(\omega_q)\mathbf{B}(\omega_q)] \Big\} - \mathrm{Tr}[\hat{\mathbf{H}}^T(\omega_q)\hat{\mathbf{H}}^*(\omega_q)\mathbf{C}(\omega_q)] - \mathrm{Tr}[\hat{\mathbf{H}}^H(\omega_q)\hat{\mathbf{H}}(\omega_q)\mathbf{D}(\omega_q)] \Big\}, \quad (71)$$

where

$$\mathbf{A}(\omega_q) = \sum_{l=1}^{L} \frac{1}{\sigma_w^2} \mathbf{x}_l(\omega_q)\mathbf{y}_l^T(\omega_q)\mathbf{U}_l, \quad (72)$$

$$\mathbf{B}(\omega_q) = \sum_{l=1}^{L} \frac{1}{\sigma_v^2} \mathbf{y}_l^*(\omega_q)\boldsymbol{f}^T(\omega_q), \quad (73)$$

$$\mathbf{C}(\omega_q) = \frac{L}{\sigma_v^2} \boldsymbol{f}^*(\omega_q)\boldsymbol{f}^T(\omega_q), \quad (74)$$

$$\mathbf{D}(\omega_q) = \sum_{l=1}^{L} \frac{1}{\sigma_w^2} \mathbf{U}_l\mathbf{y}_l^*(\omega_q)\mathbf{y}_l^T(\omega_q)\mathbf{U}_l. \quad (75)$$

Next, the maximum likelihood estimation $\hat{\mathbf{H}}(\omega_q)$ is derived by taking the partial derivative of $\ln p(\mathbf{Z}|\mathbb{H}_1)$ with respect to $\mathbf{H}^*(\omega_q)$ and ignoring the constant terms

$$\begin{aligned}
&\frac{\partial \ln p(\mathbf{Z}|\mathbb{H}_1)}{\partial \mathbf{H}^*(\omega_q)} \\
&= \frac{\partial}{\partial \mathbf{H}^*(\omega_q)} \sum_{q=0}^{Q-1} \sum_{l=1}^{L} \Big\{ - \frac{||\mathbf{y}_l(\omega_q)||^2}{\sigma_v^2} - \frac{||\mathbf{x}_l(\omega_q)||^2}{\sigma_w^2} \\
&\quad + 2\Re\Big\{ \frac{\mathbf{y}_l^T(\omega_q)\mathbf{H}^*(\omega_q)\boldsymbol{f}^*(\omega_q)}{\sigma_v^2} \\
&\quad + \frac{\mathbf{y}_l^T(\omega_q)\mathbf{U}_l\mathbf{H}^H(\omega_q)\mathbf{x}_l(\omega_q)}{\sigma_w^2} \Big\} \\
&\quad - \frac{||\mathbf{H}^*(\omega_q)\boldsymbol{f}^*(\omega_q)||^2}{\sigma_v^2} - \frac{||\mathbf{H}(\omega_q)\mathbf{U}_l\mathbf{y}_l^*(\omega_q)||^2}{\sigma_w^2} \Big\} \\
&= \frac{\partial}{\partial \mathbf{H}^*(\omega_q)} \sum_{q=0}^{Q-1} \sum_{l=1}^{L} \Big\{ - \frac{||\mathbf{y}_l(\omega_q)||^2}{\sigma_v^2} - \frac{||\mathbf{x}_l(\omega_q)||^2}{\sigma_w^2} \\
&\quad + 2\Re\Big\{ \mathrm{Tr}[\mathbf{H}^H(\omega_q)\mathbf{A}(\omega_q)] + \mathrm{Tr}[\mathbf{H}^*(\omega_q)\mathbf{B}(\omega_q)] \Big\} \\
&\quad - \mathrm{Tr}[\mathbf{H}^T(\omega_q)\mathbf{H}^*(\omega_q)\mathbf{C}(\omega_q)] \\
&\quad - \mathrm{Tr}[\mathbf{H}^H(\omega_q)\mathbf{H}(\omega_q)\mathbf{D}(\omega_q)] \Big\}. \quad (76)
\end{aligned}$$

Utilizing (61), Eq. (76) is simplified to

$$\frac{\partial \ln p(\mathbf{Z}|\mathbb{H}_1)}{\partial \mathbf{H}^*(\omega_q)} = \mathbf{A}(\omega_q) + \mathbf{B}(\omega_q) - \mathbf{C}(\omega_q)\mathbf{H}^T(\omega_q) - \mathbf{H}(\omega_q)\mathbf{D}(\omega_q). \quad (77)$$

According to (3), $\mathbf{H}(\omega_q)$ is a symmetric matrix. And letting (81) equate to zero, we obtain

$$\mathbf{C}(\omega_q)\hat{\mathbf{H}}(\omega_q) + \hat{\mathbf{H}}(\omega_q)\mathbf{D}(\omega_q) = \mathbf{A}(\omega_q) + \mathbf{B}(\omega_q), \quad (78)$$

which is solved by Hessenberg-Schur method [32]. Finally, the channel response estimation is

$$\hat{\mathbf{H}} = \mathrm{diag}[\hat{\mathbf{H}}(\omega_0), \cdots, \hat{\mathbf{H}}(\omega_{Q-1})]. \quad (79)$$

In section IV, the threshold, the false alarm probability and the detection probability are analysed using Monte-Carlo simulations.

IV. SIMULATIONS

In this section, we study the performance of the detectors using Monte-Carlo experiments where the channel response data are simulated using electromagnetic software FEKO. Two different models are considered in our simulations to analyse the influence of multipath environment complexity on the detection performance. Detection simulations include two cases. In the conventional case, we use the received echo for detection. In the time reversal case, time reversal is performed on the conventional received signal, and the time reversal echo is used to detect the target. The channel response is the superposition of the target response and the multipath response.

A. SIMULATION SETUP

In order to generate different multipath scattering environments to analyse the performance of different detectors, we construct two scattering models, where the target is a cube located at the origin with the side length of 8 meters and some six-meters spheres are used to produce multipaths. The model I, which is shown in Fig. 3(a), has 13 spheres. Model II has 2 spheres, which are shown in Fig. 3(b). And Fig. 3(c) is a top view schematic which illustrates the location relationship of target and radar transceivers. The symbols θ and ϕ in Fig. 3 are pitch and azimuth angle, respectively. Fig. 4 shows the monostatic RCS of the simulated model I. RCS is significantly large when the illumination direction ϕ is 90°. However, it is difficult to always detect the target at the angle with large RCS. Just like Fig. 3(c), in the following simulations using model I and model II, all pitch angles are set 0 degrees. Three transceivers are set and their azimuth angles are 0°, 20° and 40°, respectively.

The transmitted signal is an LFM pulse with the bandwidth of 20 MHz, the timewidth $10\mu s$ and the center frequency of 3 GHz. The number of sampling points in the frequency domain is $Q = 101$. We use Monte-Carlo experiments to illustrate the detection performance. In the case where there is no target, that is, the echo contains only noise. Monte-Carlo experiments are performed, and the detection threshold is calculated based on the false alarm probability. Then, the echo with the target is constructed, and the test statistics are calculated to obtain the detection probability. We run 100,000 independent experiments and compute the test statistics ℓ when there is no target. Then we sort these test statistics in descending order. The detection threshold is determined by the value in the sorted test statistics sequence, which located at the product of the number of Monte-Carlo experiments and the false alarm probability. For example,

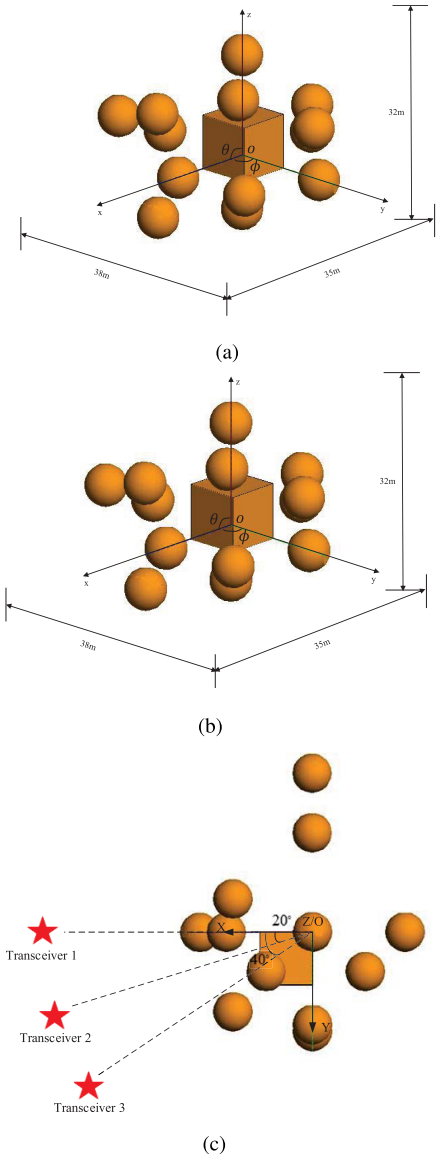

FIGURE 3. (a) Model I. (b)Model II. (c) Top view schematic of model I. The model simulated in FEKO. Target is a cube and spheres produce multipath environments.

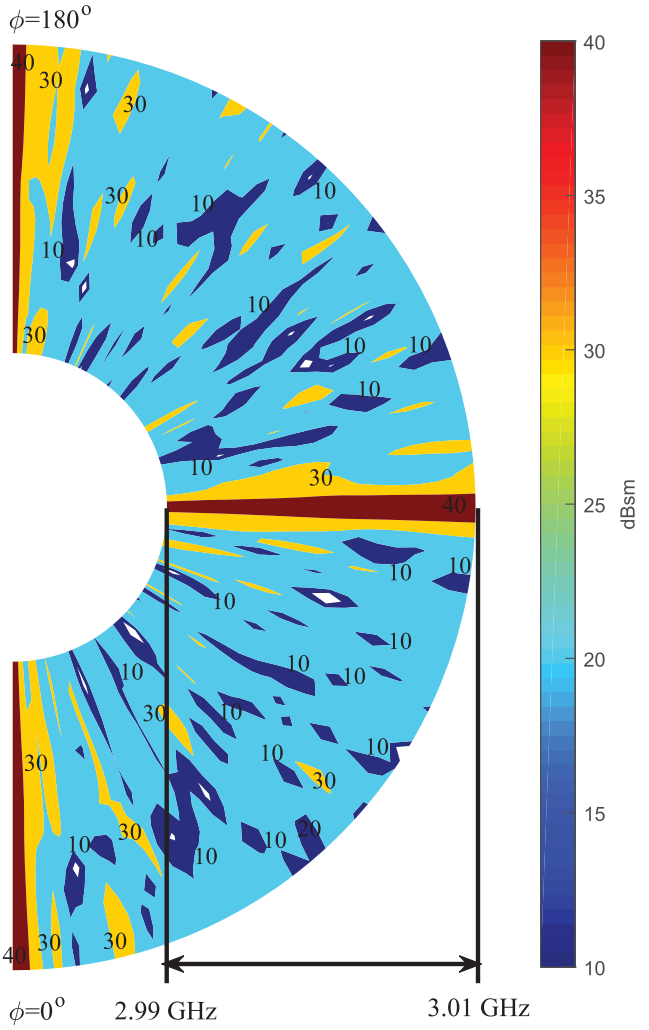

FIGURE 4. The monostatic RCS of simulated model I. The number markers represent RCS values in the fan diagram. The azimuth angle is from 0° to 180°, and the pitch angle is 0°. Frequency range is from 2.99 GHz to 3.01 GHz.

when the false alarm probability is 0.01 and Monte-Carlo experiments number is 100,000, the detection threshold is the 1000-th value in the test statistics sequence arranged in descending order. When the target exists, an echo is constructed according to (8) or (17). Then 100,000 Monte-Carlo experiments are run to calculate the test statistics and subsequently compared to the detection threshold to determine whether the target exists or not. When the test statistic exceeds the detection threshold, the target is considered to exist. The detection probability P_d is defined as the ratio of the number of experiments that target is detected to the total number of Monte-Carlo experiments.

The channel response data simulated by FEKO are noise free. Noise with different signal-to-noise ratio (SNR) is added to the data to study the relationship between the detection probability and the SNR. For the j-th transmitter and the i-th receiver, the SNR is defined as

$$\mathrm{SNR}_{ij} = \frac{\sum_{q=0}^{Q-1} |H_{ij}(\omega_q)F_j(\omega_q)|^2}{Q\sigma_v^2}. \tag{80}$$

Note that the definition of SNR in (80) is different from the definition of a point target. In our paper, the ratio of average target power to noise in the detection window is used as the SNR. Generally, the radar working environment does not change in a short time, which causes the noise power to be constant. Here, we assume $\sigma_v^2 = \sigma_w^2 = 1$. SNR is defined based on the echo signal in the conventional case. According to (80), SNR is changed by adjusting the transmitted signal power with the determined noise power and the channel response. In the ideal TR situation, although in the conventional step, the virtual transmission is performed because the channel response is known, the power of the transmitted signal can still be calculated by the SNR defini-

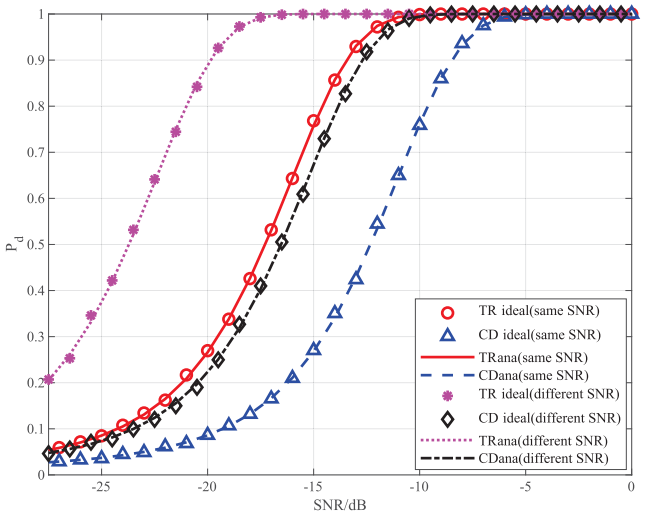

FIGURE 5. The detection probability P_d versus SNR under ideal scenario when SNR of each channel is different. We use the scattering model I with two transceivers and four propagation channels. In order to unify the representation, the average SNR of all channels are used as the x-axis.

tion in (80), which is consistent with the ideal conventional situation. In the realistic time reversal case, the radar receives echoes twice, each of which contains different noises. In this case, SNR is defined using conventional echo.

We set the false alarm probability $P_{fa} = 0.01$. For the single transceiver radar, it is set at the location of $\phi = 20°$. When the number of transceivers is 2, transceivers locate at $\phi = 0°$ and $\phi = 20°$. And when the transceivers number is 3, transceivers with $\phi = 0°, 20°, 40°$ are used. We utilize digital sequences 1, 2 and 3 to indicate the number of transceivers. In the following description, the CD is used to represent the conventional method and TR is used to represent the time reversal method. For the ideal scenario, the snapshot is 1. For the realistic scenario, we use 1 snapshot data to analyse the TR detectors performance and 2 snapshots data to analyse the conventional detectors. For the ideal scenario, lines represent theoretical values while markers refer to Monte-Carle results. For the realistic scenario, Monte-Carlo results are depicted.

B. SIMULATION RESULTS

1) IDEAL SCENARIO

Fig. 5 shows the detection probability curve versus SNR with two distributed transceivers used. For multistatic radars, the channels corresponding to each transceiver are usually inconsistent, which results in different multipath scattering environments for each channel and causes differences in SNR between the channels. The scattering model I is used in this simulation. Two cases are considered to study the relationship between SNR of the channels and the detection probability. In case 1, we assume that SNR is the same for each channel. In case 2, we assume that SNR is different with respect to the different channels, specifically, $\mathrm{SNR}_{11} = \mathrm{SNR}_{22} = \mathrm{SNR}_{12} - 3\,\mathrm{dB} = \mathrm{SNR}_{21} - 3\mathrm{dB}$. In order to uniformly represent the detectors performance of different SNR of channels, the x-axis in Fig. 5 is expressed by the average of all channels SNR. The Monte-Carlo results are consistent with the theoretical results. For case 2 with different channel SNR, because half of the number of channels have higher SNR than the other case, better detection performance is achieved. TR detector in case 2 has a SNR gain about 6 dB over the detector in case 1, which is consistent with the difference of the channel SNR. For case 1, i.e. the same channel SNR situation, comparing with conventional detector, SNR gain of time reversal detector is about 4.9 dB. And for case 2 with different channel SNR, time reversal detector has SNR gain about 7.2 dB. When the multipath scattering of some channels is more intense, the corresponding channel SNR will also improve, which results in a higher detection probability with more multipath exploited.

Fig. 6 displays the results of the different number of transceivers when SNR of each channel is the same. For a single transceiver, its derivation is described in [24]. It is obvious that as the number of transceivers increases, the detection probability improves because more transceivers bring more target information. Compared with the conventional detector, SNR gain for TR detector of the single transceiver is about 2.7 dB and for 2 transceivers and 3 transceivers, SNR gain are about 4.9 dB and 3.8 dB, respectively. SNR gain is related to the channel response. However, SNR gain is not directly proportional to the number of radar transceivers. Since different transceivers corresponding to their respective multipath scattering environments, this results in the inconsistency of the multipath that each transceiver can be exploited.

Fig. 7 illustrates the influence of different multipath environments on the performance of detectors. For the TR detector, the detection probability under model I which has more scatters is higher than the detection probability under model II. For the conventional detector, the detection probability under model II is higher than the other model. Compared with conventional detectors, the corresponding SNR gains of the TR detectors in model I and model II are 3.8 dB and 3.6 dB, respectively. This phenomenon indicates that multipaths have a detrimental effect on the conventional detection method. TR detector can take advantage of this adverse impact and convert the multipath influence into favorable factors to improve the detection probability.

Although according to our definition at a low SNR, the target energy in the detection window can be accumulated of multiple frequency points and multiple channels to achieve detection.

2) REALISTIC SCENARIO

Fig. 8 depicts the detection probability curves for the TR-GLRT and CD-GLRT detection problems when the number of transceivers is two. SNR is consistent with the situations in Fig. 5 with two cases. Compared with the conventional detector, TR detector has a gain about 2.5 dB in case1 and 3.2 dB in case 2. SNR gain of realistic scenario is less than ideal scenario because channel response is unknown. Then we analyse the TR detector performance of two cases.

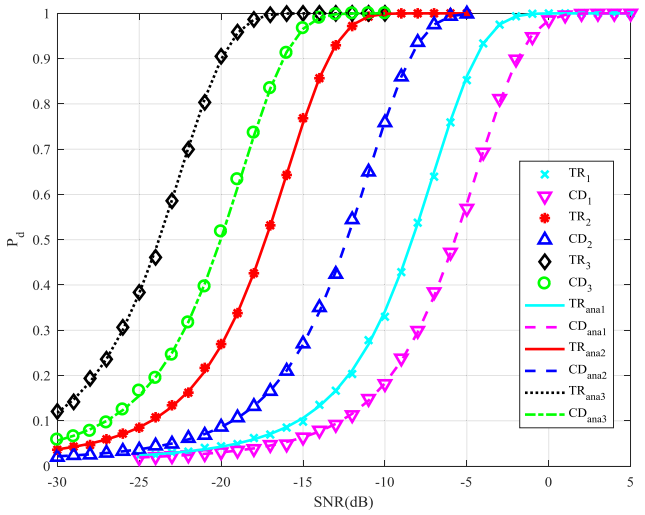

FIGURE 6. The detection probability P_d versus SNR under ideal scenario while the number of transceivers is different. We use scattering model I to analyse. The number of transceivers are 1, 2 and 3, respectively. SNR of each channel is the same.

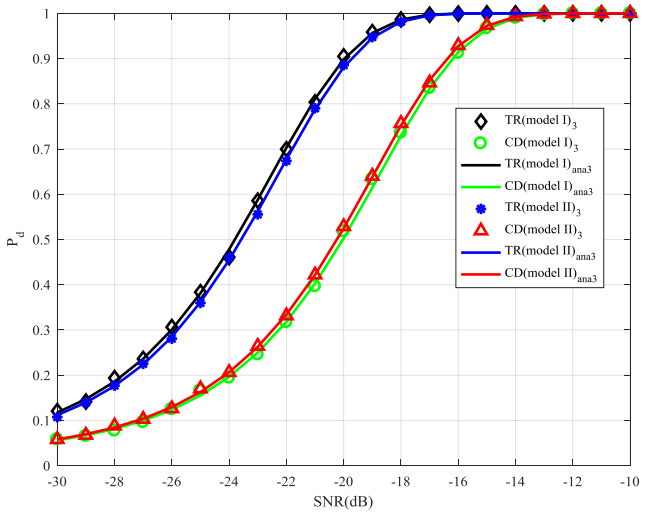

FIGURE 7. The detection probability P_d versus SNR under different scattering models. The number of transceivers is three. SNR of each channel is the same.

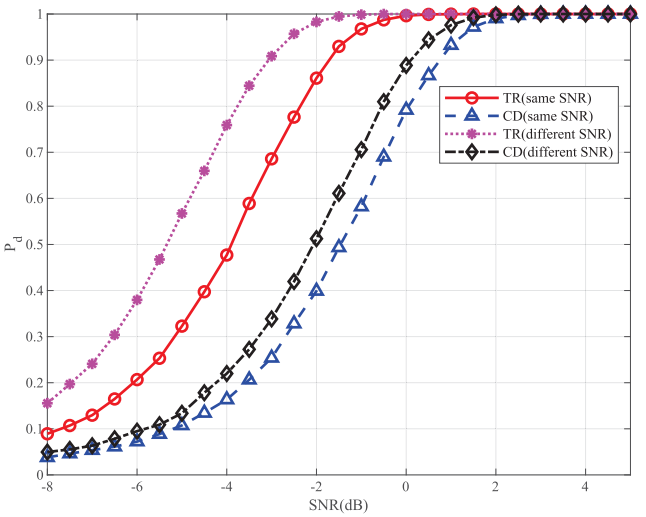

FIGURE 8. The detection probability P_d versus SNR under realistic scenario when the SNR of channels are different. Model I with two transceivers is used in this simulation analysis. We use the average SNR of all channels as the x-axis.

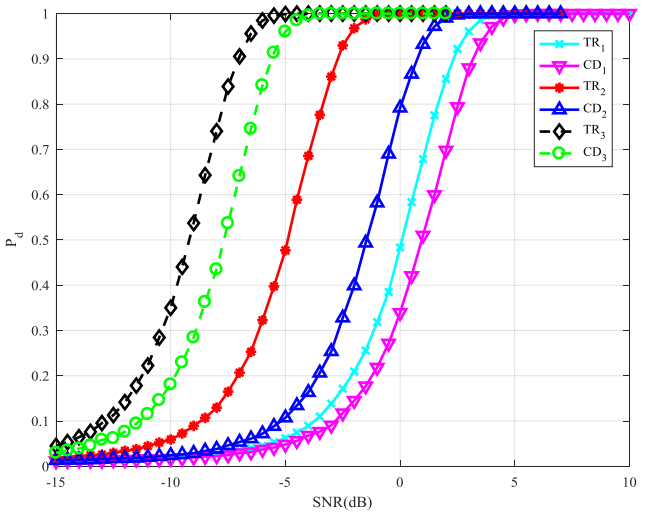

FIGURE 9. The detection probability P_d versus SNR under realistic scenario for different number of transceivers. We use Model I to analyse. The number of transceivers are 1, 2 and 3. Each of channel SNR is the same.

Although the average SNR difference of each channel is 1.5 dB, the difference between two TR detection results is about 1.2 dB. In the realistic scenario, the multipath cannot be fully utilized for the channel obtained by the maximum likelihood estimation, which is not as good as when the channel is known in the ideal scenario.

Fig. 9 illustrates the curves of the detection probability versus SNR under the realistic scenario when the number of transceivers is different. The derivation of a single transceiver is introduced in [24]. The results show that more transceivers lead to higher detection probability. For the number of transceivers of 1, 2 and 3, the SNR gain are 0.9 dB, 3.5 dB and 1.5 dB, respectively. Though the channel response is the same as Fig. 6, SNR gain is less than the ideal scenario because maximum likelihood estimation is used to detect the target in the realistic scenario. Notice that SNR gain has no relationship with the number of radar transceivers, but is related to the channel response, i.e. the situation of multipath exploitation.

Fig. 10 shows that different multipath environments affect the detection performance in the realistic scenario. Compared with the ideal scenario in Fig. 7, the difference of TR detector performance is more obvious between different models. For model I, SNR gain of TR detector over conventional detector is about 1.5 dB. For the other model, SNR gain is about 1 dB. The TR detector in model I has a 0.2 dB SNR gain over the other model. However, the performance of the conventional

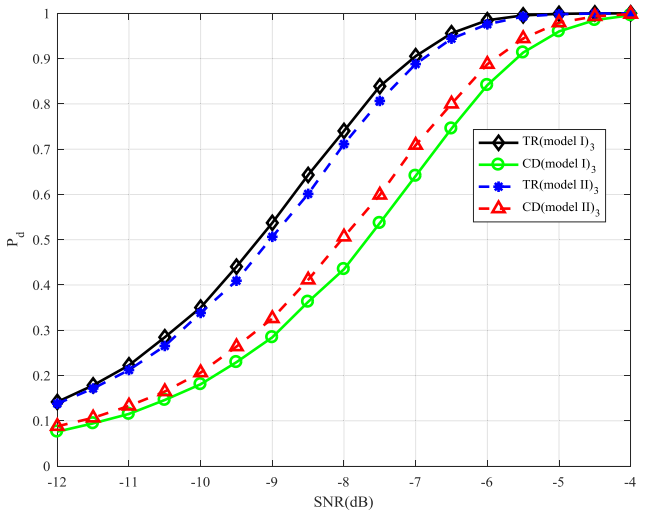

FIGURE 10. The detection probability P_d versus SNR under realistic scenario for different scattering models when the number of radar transceivers is three. We use Model I and model II to analyse. Each of channel SNR is the same.

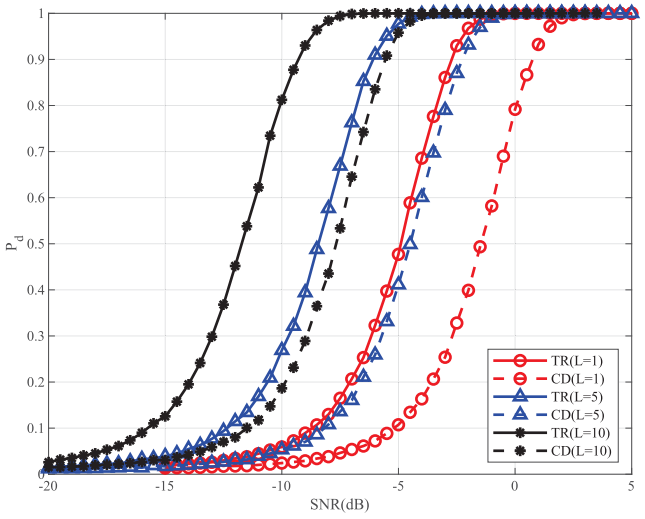

FIGURE 11. The detection probability P_d versus SNR under realistic scenario for different snapshots when the number of radar transceivers is two. We use Model I to analyse. Each of channel SNR is the same.

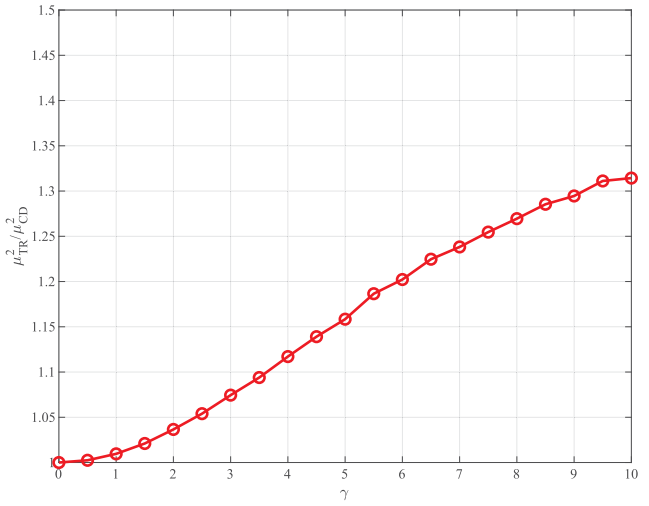

FIGURE 12. The performance gain versus multipath variance. Two transceivers are employed.

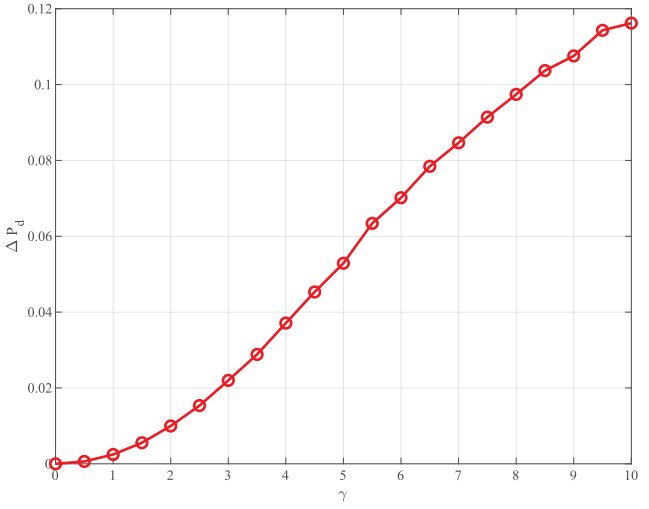

FIGURE 13. The difference of detection probability P_d versus multipath intensity.

detector is 0.3 dB lower than the detector in model II. More multipaths exploitation will improve the TR detection probability and degrade the performance of conventional detector.

Fig. 11 depicts the effect of the number of snapshots on the detection probability. It is obvious that more snapshots will improve the detection performance since more multipaths are utilized.

3) DETECTION PERFORMANCE GAIN

Although Fig. 7 and Fig. 10 demonstrate that multipath has a beneficial effect on TR detection, we also use a numerical method to illustrate the detection performance gain due to the exploitation of multipath by TR. We study the performance gain of the TR detector over the conventional detector when the channel response is known. The TR and conventional detectors are shown in (30) and (46), respectively, which have similar forms. The detection probability of these two detectors is only controlled by μ_{CD} and μ_{TR} with the same false alarm probability and noise power. Therefore, we can compare the performance of two detectors by calculating the ratio of μ_{TR}^2 and μ_{CD}^2 [24]

$$\frac{\mu_{\mathrm{TR}}^2}{\mu_{\mathrm{CD}}^2} = \frac{||\mathbf{H}\bar{\mathbf{U}}\mathbf{H}^*\boldsymbol{f}^*||^2}{||\mathbf{H}\boldsymbol{f}||^2} \geq 1. \tag{81}$$

Considering a special case of a point target, and there is no multipath in the scattering environment, that is, the amplitude of each channel is a constant, i.e. $\forall q, |H(\omega_q)| = \alpha, \alpha \geq 0$. Under this condition, the equal sign holds in (81). A rich multipath environment can cause large variances in the channel response, which will lead to the TR detector to outperform the conventional detector [24].

We generate a random channel that satisfies the complex Gaussian distribution to study the effect of multipath on the performance gain of the TR detector. We define that [26]

$$H(\omega_q) \sim \mathcal{CN}(\alpha, \gamma^2), \tag{82}$$

where γ^2 represents the intensity of the multipath scattering. Fig. 12 depicts the performance of TR and conventional detectors with varying multipath intensity. Fig. 13 illustrates the difference of the detection probability of TR and conventional detectors, i.e. the y-axis is defined as $\Delta P_d = P_{d,\mathrm{TR}} - P_{d,\mathrm{CD}}$. It is straightforward to know that as the multipath intensity increases, the detection performance improves significantly.

V. CONCLUSION

In this paper, the time reversal detection problem in the multistatic radar system with multipaths has been studied. We have derived the conventional detectors and the time reversal detectors for both the ideal and the realistic scenarios. The TR detectors utilize the time reversal technique to realize the spatial and temporal focusing by matching propagation channels and obtain better detection performance than the conventional detectors. We have constructed two scattering models with different channel responses and used Monte-Carlo experiments to validate the detection problem. The experiment results show the superiority of the TR detectors. And more complex multipath environments produce more multipaths, which bring to a higher detection probability. In addition, the results show that more radar transceivers will bring more target information and therefore lead to better detection performance.

REFERENCES

[1] J. Liu, H. Li, and B. Himed, "Two target detection algorithms for passive multistatic radar," *IEEE Trans. Signal Process.*, vol. 62, no. 22, pp. 5930–5939, Nov. 2014.
[2] P. Wang, H. Li, and B. Himed, "Moving target detection using distributed MIMO radar in clutter with nonhomogeneous power," *IEEE Trans. Signal Process.*, vol. 59, no. 10, pp. 4809–4820, Oct. 2011.
[3] G. Sun, W. Zhang, J. Tong, Z. He, and Z. Wang, "Knowledge-aided target detection for multistatic passive radar," *IEEE Access*, vol. 7, pp. 53463–53475, 2019.
[4] S. Sirianunpiboon, S. D. Howard, and D. Cochran, "A Bayesian derivation of generalized coherence detectors," in *Proc. IEEE Int. Conf. Acoust., Speech Signal Process. (ICASSP)*, Mar. 2012, pp. 3253–3256.
[5] X. Zhang, J. Sward, H. Li, A. Jakobsson, and B. Himed, "A sparsity-based passive multistatic detector," *IEEE Trans. Aerosp. Electron. Syst.*, vol. 55, no. 6, pp. 3658–3666, Dec. 2019.
[6] Y. Yang, H. Su, Q. Hu, S. Zhou, and J. Huang, "Centralized adaptive CFAR detection with registration errors in multistatic radar," *IEEE Trans. Aerosp. Electron. Syst.*, vol. 54, no. 5, pp. 2370–2382, Oct. 2018.
[7] X. Zeng, M. Yang, B. Chen, and Y. Jin, "Estimation of direction of arrival by time reversal for low-angle targets," *IEEE Trans. Aerosp. Electron. Syst.*, vol. 54, no. 6, pp. 2675–2694, Dec. 2018.
[8] H. Xiang, B. Chen, M. Yang, T. Yang, and D. Liu, "A novel phase enhancement method for low-angle estimation based on supervised DNN learning," *IEEE Access*, vol. 7, pp. 82329–82336, 2019.
[9] T. A. Seliga and F. J. Coyne, "Multistatic radar as a means of dealing with the detection of multipath false targets by airport surface detection equipment radars," in *Proc. IEEE Radar Conf.*, May 2003, pp. 329–336.
[10] R. Linnehan and J. Schindler, "Multistatic scattering from moving targets in multipath environments," in *Proc. IEEE Radar Conf.*, 2009, pp. 1–6.
[11] J. Liu, W. Liu, C. Hao, and C. Orlando, "Persymmetric subspace detectors with multiple observations in homogeneous environments," *IEEE Trans. Aerosp. Electron. Syst.*, early access, Jan. 20, 2020, doi: 10.1109/TAES.2020.2967244.
[12] W. Liu, J. Liu, Y. Gao, G. Wang, and Y.-L. Wang, "Multichannel signal detection in interference and noise when signal mismatch happens," *Signal Process.*, vol. 166, Jan. 2020, Art. no. 107268.
[13] H. T. Hayvaci, A. De Maio, and D. Erricolo, "Improved detection probability of a radar target in the presence of multipath with prior knowledge of the environment," *IET Radar, Sonar Navigat.*, vol. 7, no. 1, pp. 36–46, Jan. 2013.
[14] U. Kumbul and H. T. Hayvaci, "Multipath exploitation for knowledge-aided adaptive target detection," *IET Radar, Sonar Navigat.*, vol. 13, no. 6, pp. 863–870, Jun. 2019.
[15] A. Aubry, A. De Maio, G. Foglia, and D. Orlando, "Diffuse multipath exploitation for adaptive radar detection," *IEEE Trans. Signal Process.*, vol. 63, no. 5, pp. 1268–1281, Mar. 2015.
[16] Y. Rong, A. Aubry, A. De Maio, and M. Tang, "Diffuse multipath exploitation for adaptive detection of range distributed targets," *IEEE Trans. Signal Process.*, vol. 68, pp. 1197–1212, 2020.
[17] S. Sen and A. Nehorai, "Adaptive OFDM radar for target detection in multipath scenarios," *IEEE Trans. Signal Process.*, vol. 59, no. 1, pp. 78–90, Jan. 2011.
[18] M. Fink, C. Prada, F. Wu, and D. Cassereau, "Self focusing in inhomogeneous media with time reversal acoustic mirrors," in *Proc. IEEE Ultrason. Symp.*, Oct. 1989, pp. 681–686.
[19] Y. Jin, J. M. F. Moura, Y. Jiang, D. D. Stancil, and A. G. Cepni, "Time reversal detection in clutter: Additional experimental results," *IEEE Trans. Aerosp. Electron. Syst.*, vol. 47, no. 1, pp. 140–154, Jan. 2011.
[20] M. Fink, "Time reversal of ultrasonic fields. I. basic principles," *IEEE Trans. Ultrason., Ferroelectr., Freq. Control*, vol. 39, no. 5, pp. 555–566, Sep. 1992.
[21] N. Chakroun, M. A. Fink, and F. Wu, "Time reversal processing in ultrasonic nondestructive testing," *IEEE Trans. Ultrason., Ferroelectr., Freq. Control*, vol. 42, no. 6, pp. 1087–1098, Nov. 1995.
[22] G. Lerosey, J. de Rosny, A. Tourin, A. Derode, G. Montaldo, and M. Fink, "Time reversal of electromagnetic waves," *Phys. Rev. Lett.*, vol. 92, no. 19, May 2004, Art. no. 194301.
[23] K. Sarabandi, I. Koh, and M. D. Casciato, "Demonstration of time reversal methods in a multi-path environment," in *Proc. IEEE Antennas Propag. Soc. Symp.*, Jun. 2004, pp. 4436–4439.
[24] J. M. F. Moura and Y. Jin, "Detection by time reversal: Single antenna," *IEEE Trans. Signal Process.*, vol. 55, no. 1, pp. 187–201, Jan. 2007.
[25] Y. Jin and J. M. F. Moura, "Time-reversal detection using antenna arrays," *IEEE Trans. Signal Process.*, vol. 57, no. 4, pp. 1396–1414, Apr. 2009.
[26] Y. Jin, J. M. F. Moura, and N. O'Donoughue, "Time reversal in multiple-input multiple-output radar," *IEEE J. Sel. Topics Signal Process.*, vol. 4, no. 1, pp. 210–225, Feb. 2010.
[27] F. Foroozan and A. Asif, "Time-reversal ground-penetrating radar: Range estimation with Cramér–Rao lower bounds," *IEEE Trans. Geosci. Remote Sens.*, vol. 48, no. 10, pp. 3698–3708, Oct. 2010.
[28] A. G. Cepni, D. D. Stancil, B. Henty, Y. Jiang, Y. Jin, J. M. F. Moura, and J.-G. Zhu, "Experimental results on single antenna target detection using time-reversal techniques," in *Proc. IEEE Antennas Propag. Soc. Int. Symp.*, Jul. 2006, pp. 703–706.
[29] J. M. F. Moura, Y. Jin, D. Stancil, J.-G. Zhu, A. Cepni, Y. Jiang, and B. Henty, "Array processing using time reversal: Experiments and performance," in *Proc. IEEE Int. Conf. Acoust. Speed Signal Process.*, May 2006, pp. 1053–1056.
[30] J. M. F. Moura and Y. Jin, "Time reversal imaging by adaptive interference canceling," *IEEE Trans. Signal Process.*, vol. 56, no. 1, pp. 233–247, Jan. 2008.
[31] X. Zhang, *Matrix Analysis and Applications*, 1st ed. Beijing, China: Qsinghua, 2004.
[32] G. Golub, S. Nash, and C. Van Loan, "A hessenberg-schur method for the problem AX + XB= C," *IEEE Trans. Autom. Control*, vol. 24, no. 6, pp. 909–913, Dec. 1979.

ZHAOMING ZHANG received the B.S. degree from Xidian University, China, in 2017, where he is currently pursuing the Ph.D. degree with the National Laboratory of Radar Signal Processing.

His current research interests include time reversal technology, and radar target detection and classification.

BAIXIAO CHEN was born in Anhui, China, in 1966. He received the degree from the Metallurgy College, East China, in 1987, and the master's degree in circuit and system and the Ph.D. degree in signal and information processing from Xidian University, in 1994 and 1997, respectively. Since then, he has been a Faculty Member with the National Laboratory of Radar Signal Processing. He has worked with the Metallurgy College, from July 1987 to July 1991. He has worked as a Lecturer and an Associate Professor, from October 1997 to May 1999 and June 1996 to May 2003, respectively. In 2006, he was selected into the New Century Elitist Support Program of the Ministry of Education. He is currently a Professor of signal and information processing. His general research interests include radar signal processing, new radar system design, array signal processing, and precise guidance.

MINGLEI YANG (Member, IEEE) received the B.E. degree in electronic engineering and the Ph.D. degree in signal and information processing from Xidian University, China, in 2004 and 2009, respectively. Since 2009, he has been working with the National Laboratory of Radar Signal Processing, Xidian University, where he is currently an Associate Professor. From 2014 to 2015, he was a Visiting Scholar with the Elisha Yegal Bar-Ness Center for Wireless Communications and Signal Processing Research (CWCSPR), New Jersey Institute of Technology (NJIT). He has been doing research in the fields of array signal processing, MIMO signal processing, and polarization information processing. He has published more than 60 peer-reviewed journals and conference papers and more than 40 inventions.